Where do the Two Cores of the Irminger Current Come From? A Lagrangian Study Using a 1/10° Ocean Model Simulation

Fried, Nora; Katsman, Caroline A.; de Jong, M. F.

DOI
10.1029/2023JC020713

Publication date
2024

Document Version
Final published version

Published in
Journal of Geophysical Research: Oceans

Citation (APA)
Fried, N., Katsman, C. A., & de Jong, M. F. (2024). Where do the Two Cores of the Irminger Current Come From? A Lagrangian Study Using a 1/10° Ocean Model Simulation. *Journal of Geophysical Research: Oceans*, *129*(10), Article e2023JC020713. https://doi.org/10.1029/2023JC020713

JGR Oceans

RESEARCH ARTICLE
10.1029/2023JC020713

Where do the Two Cores of the Irminger Current Come From? A Lagrangian Study Using a 1/10° Ocean Model Simulation

Nora Fried[1], **Caroline A. Katsman**[2], **and M. F. de Jong**[1]

[1]Department of Ocean Systems, NIOZ, Royal Netherlands Institute for Sea Research, Texel, The Netherlands, [2]Delft University of Technology, Faculty of Civil Engineering and Geosciences, Department of Hydraulic Engineering, Delft, The Netherlands

Abstract The Irminger Current (IC) brings relatively warm and saline waters northward in the North Atlantic subpolar gyre, contributing to the upper limb of the Atlantic Meridional Overturning Circulation. The IC is a two-core current with surface-intensified velocities. The eastern core, closest to the Reykjanes Ridge, is warmer and more saline than the western core. To investigate the source waters of the two IC cores, using a 1/10° ocean model, we track Lagrangian particles released in the IC at OSNAP East (~59.5°N) in the upper 1,000 m backward in time for one model year. Over a 1-year time scale, nearly all particles are sourced from nearby regions of the Irminger Sea and Iceland Basin. Those seeded in the western IC core mostly originate from the Irminger Sea (83%), while those in its eastern core mostly originate from the Iceland Basin (69%). Iceland Basin water feeding the IC predominantly crosses the Reykjanes Ridge near 57°N and 59°N. Generally, particles from the Irminger Sea are colder and fresher than particles from the Iceland Basin. The fraction of waters from the Iceland Basin and the Irminger Sea varies from month to month. So, to explain monthly variations of the two IC cores at the OSNAP East line, changes in hydrographic properties in both basins as well as their contributions must be considered. Based on this model study, we interpret the Irminger Sea circulation as a basin-wide recirculation with an increasing contribution of Iceland Basin waters toward the ridge which is subject to monthly variations.

Plain Language Summary The Irminger Current (IC) brings warm and saline waters northward along the western side of the Mid Atlantic Ridge. The IC is a two-core current where the eastern core is warmer and more saline than the western core. Here, we investigate the sources of the IC with a focus on the different water mass properties of the two cores to understand the observed transport variability of the IC. We release virtual particles in the IC in an ocean model simulation with a 1/10° resolution and track their paths backward in time for 1 year. We find that the western core has its main source in the Irminger Sea with colder and fresher properties while the eastern core is mostly fed by warmer and more saline waters from the Iceland Basin. The mix of waters from the Iceland Basin and the Irminger Sea varies from month to month. So, to explain monthly variations of the two IC cores at the OSNAP East line, this model suggests that changes in hydrographic properties in both basins as well as their contributions must be considered.

Key Points:

- Both Irminger Current (IC) cores at 59.5°N are fed by the Irminger Sea and Iceland Basin, with more Irminger water in the western core
- Iceland Basin water feeding the IC at that latitude predominantly crosses the Reykjanes Ridge near 57°N and 59°N
- The ratio of waters from the two basins varies on a monthly time scale which may lead to hydrographic and transport variability in the IC

Supporting Information:

Supporting Information may be found in the online version of this article.

Correspondence to:

N. Fried,
nora.fried@nioz.nl

Citation:

Fried, N., Katsman, C. A., & de Jong, M. F. (2024). Where do the two cores of the Irminger current come from? A Lagrangian study using a 1/10° ocean model simulation. *Journal of Geophysical Research: Oceans*, *129*, e2023JC020713. https://doi.org/10.1029/2023JC020713

Received 14 NOV 2023
Accepted 13 SEP 2024

Author Contributions:

Conceptualization: Caroline A. Katsman, M. F. de Jong
Formal analysis: Nora Fried
Investigation: Nora Fried
Methodology: Nora Fried
Supervision: Caroline A. Katsman, M. F. de Jong
Writing – original draft: Nora Fried
Writing – review & editing: Caroline A. Katsman, M. F. de Jong

1. Introduction

The Atlantic Meridional Overturning circulation (AMOC) is a key component of the earth's climate system. Earlier studies already pointed at the importance of the Irminger Sea for deep convection relevant to AMOC (Pickart et al., 2003; Våge et al., 2011; van Aken et al., 2011). More recently, results from the Overturning in the Subpolar North Atlantic Program (OSNAP, Chafik & Rossby, 2019; Fu et al., 2023; Li et al., 2021; Lozier et al., 2017, 2019; Petit et al., 2020) have shown that most of the mean overturning in the subpolar North Atlantic and its variability (82%) arises from the eastern subpolar North Atlantic (OSNAP East, 16.8 Sv), and not from the Labrador Sea (OSNAP West, 2.6 Sv) as previously thought. OSNAP measures the boundary currents across the whole subpolar gyre with mooring arrays by recording velocity, temperature, and salinity. The recently updated 6-year OSNAP time series highlights the seasonal cycle of the overturning strength in the subpolar North Atlantic calculated with respect to the 27.55 - isopycnal, characterized by a peak-to-peak difference of 9.0 Sv with a maximum in late spring and a minimum in early winter (Fu et al., 2023). The seasonality can be explained by wintertime transformation and export of dense water modulated by seasonally varying Ekman transport (Fu

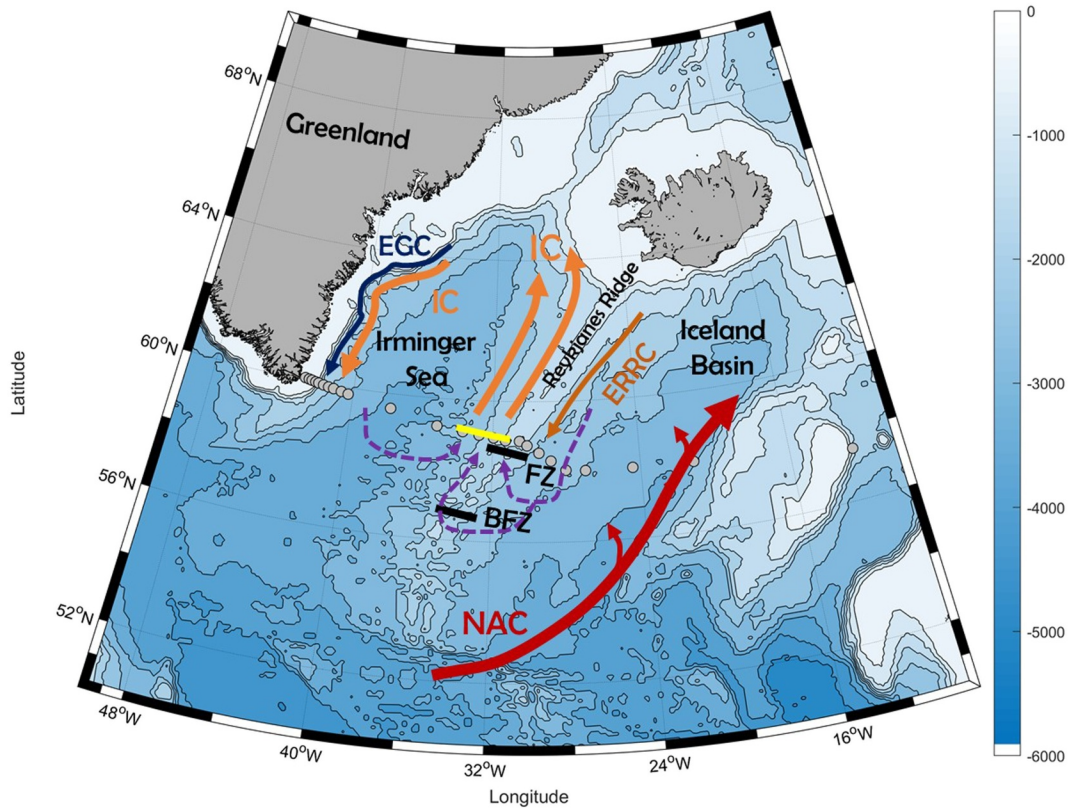

Figure 1. Circulation in the eastern subpolar North Atlantic with focus on the Irminger Sea and Iceland Basin. Currents, circulation and topographic features depicted here: North Atlantic Current (NAC, red), East Reykjanes Ridge Current (ERRC, dark orange), Irminger Current (IC, orange), East Greenland Current (EGC, blue), Bight Fracture Zone (BFZ), second unnamed fracture zone (FZ). Gray circles: OSNAP East moorings. Yellow line: particle release line. Underlying bathymetry is model bathymetry from the POP ocean model configuration at 1/10° resolution. Purple colors illustrate possible pathways investigated in this study.

et al., 2023). The observations available from OSNAP provide new information on the mean state and variability of the AMOC in the subpolar North Atlantic across multiple time scales, but the variability and pathways of the contributing currents are not yet fully understood.

In this study, we focus on the Irminger Current (IC), which is a contributor to the AMOC's upper limb bringing warm and saline waters northward along the western side of the Reykjanes Ridge (RR, Figure 1, de Jong et al., 2020; Fried & de Jong, 2022, Petit et al., 2019; Våge et al., 2011). The IC is part of the cyclonic Irminger Sea circulation (Krauss, 1995; Reverdin et al., 2003) and continues southward off the east Greenland shelf alongside the East Greenland Current (EGC). After rounding Cape Farewell, the EGC/IC continues as the West Greenland Current (Cuny et al., 2002; de Jong et al., 2014; Pacini et al., 2023).

The IC has been described using mooring observations along the OSNAP East line (Figure 1; de Jong et al., 2020; Fried & de Jong, 2022) and hydrographic sections along both the OSNAP and the OVIDE line (Chafik et al., 2014; Knutsen et al., 2005; Lherminier et al., 2007; Mercier et al., 2015). Here, the IC is a surface-intensified two-core current flowing northward with a weak southward flow at intermediate depth between the two cores (de Jong et al., 2020; Fried & de Jong, 2022; Våge et al., 2011). The two cores are characterized by different water mass properties: the eastern core is warmer and more saline than the western core (de Jong et al., 2020; Petit et al., 2019; Våge et al., 2011). The reason for the difference in water mass properties within the IC is still unknown.

The flow across RR has been investigated by Petit et al. (2019) who used hydrographic ship sections and mooring observations to investigate the connectivity of the IC and East Reykjanes Ridge Current (ERRC) over the ridge and between the two basins. Based on a budget analysis, they proposed an additional contribution to the IC from

the Irminger Sea and the Labrador Sea, with the latter being the larger contribution. They found that south of 59.5°N the IC consists of waters from the western subpolar gyre in addition to the westward cross-ridge flow. North of 59°N they find that the IC is fed by two cross-ridge flows from the Iceland Basin.

The crossing of waters from the Iceland to the Irminger Basin has also been investigated by Koman et al. (2020) using ARGO and altimetry with a focus on the fate of the waters in the ERRC. Combined with the study of Petit et al. (2018) using hydrographic sections along the OVIDE line they find that waters from the Iceland Basin enter the Irminger Sea through the Bight Fracture Zone at 57°N and smaller fracture zones in the ridge around 59°N (FZ in Figure 1, just south of the OSNAP line). The westward flow through the BFZ toward the Irminger Sea has also been identified by Bower et al. (2002) using acoustically tracked floats.

In this paper, we study the near-field sources of the IC in a Lagrangian framework. We investigate whether different sources of the two IC cores may help explain the differences in temperature and salinity characteristics seen at the IC mooring array (de Jong et al., 2020; Fried & de Jong, 2022). To do so, we release Lagrangian particles in a high-resolution ocean model simulation at the location of the IC moorings and track them backwards in time for 1 year.

In Section 2 we introduce the ocean model simulation, validate it against two observational products in the region of interest, and detail the Lagrangian tracking strategy. Our study focuses on identifying potentially different pathways into the two IC cores based on the particle density distribution, and on connections between the Irminger Sea and Iceland Basin on different temporal scales by analyzing particle travel times (Section 3). In Section 4, we investigate the existence of preferred pathways across the Reykjanes Ridge toward the IC mooring array and the temporal variability of those pathways for each core. Section 5 focuses on the water mass properties carried by the two IC cores based on their sources in the Irminger Sea and Iceland Basin. Finally, Section 6 summarizes the results, draws conclusions, and gives an outlook for further research.

2. Data and Methods

To investigate the sources of the two IC cores we follow a Lagrangian approach. Using 1 year of velocity data from a global ocean model simulation, we track virtual particles and their hydrographic properties along their track using the Lagrangian tracking software OceanParcels (Delandmeter & Van Sebille, 2019). In the following subsections we first introduce the configuration of the ocean model simulation (Section 2.1). We validate the output from the global ocean model simulation against observations described in Section 2.2. The set-up of the Lagrangian Particle tracking simulation in OceanParcels is described in Section 2.3.

2.1. POP Ocean Model Simulation

The velocity field used to advect the particles in our Lagrangian study is obtained from a simulation with the Parallel Ocean Program ocean-only model (POP), described in detail by Weijer et al. (2012). This simulation uses a tripolar B-grid with a nominal horizontal resolution of 1/10°. In the Irminger Sea and the Iceland Basin, the resolution required to resolve the baroclinic Rossby deformation radius is typically 1/8°–1/16° (Hallberg, 2013, their Figure 1). This model configuration can therefore be considered eddy-permitting in the area of interest. In the vertical, POP has 42 layers of increasing thickness ranging from 5 m at the surface to 250 m at depth.

This POP simulation is driven by repeated COREv2-NYF climatological normal-year atmospheric forcing (Griffies et al., 2009; Large & Yeager, 2009). Consequently, all simulated variability is attributable to internal ocean processes, apart from seasonal time scales induced by the forcing. Ocean convection is parametrized using the KPP parametrization (Large et al., 1994), strongly increasing vertical viscosities and diffusivities whenever an unstable stratification arises. In the horizontal, biharmonic viscosity and diffusion are applied. The model simulation is initialized with interpolated temperature and salinity fields from the annual mean WOCE Global Hydrographic Climatology (Gouretski & Koltermann, 2004) and spun up from rest. During the first 75 years of the spin-up phase, the surface salinity is weakly restored to climatology to suppress salinity drift (Weijer et al., 2012). During model years 71–75 of this spin up-phase, the applied restoring flux is explicitly diagnosed, and used to formulate mixed boundary conditions that are applied in the remainder of the simulation. From model year 76 onwards, the surface salinity is no longer restored but forced by a surface flux corresponding to the monthly climatology of this diagnosed 5-year restoring flux. Throughout the entire simulation, the sea-ice edge is

fixed and defined using the −1.8°C isoline of the sea surface temperature climatology. Temperature and salinity under the sea ice are restored with a time scale of 30 days.

To constrain the required data storage capacity, for the full 1/10° POP simulation only monthly mean model output was saved. As high-frequency model output is needed for our Lagrangian particle tracking study, a single model year well after the spin-up phase was repeated, and snapshots of this repeated part of the model simulation were saved at a daily frequency. As the atmospheric forcing is the same for every model year, we expect that the characteristics of this 1-year simulation are not sensitive to the choice of model year.

2.2. Comparison Between POP and Observations

To assess that the POP model simulation has sufficient skill in the Irminger Sea, we compare it to two additional data sets: the OSNAP data (https://www.o-snap.org/data-access/) and the reanalysis product from CMEMS (Copernicus Marine Environment Monitoring Services, http://marine.copernicus.eu, E.U. Copernicus Marine Service Information, https://doi.org/10.48670/moi-00021).

As the POP simulation used in this study is forced by normal-year atmospheric forcing (Section 2.1), it is expected to be more comparable to a multi-year average than to an individual reanalysis year or observational year. Hence, we compare the 1-year average of model output from POP to the 2014–2020 OSNAP data and the 2014–2020 average of CMEMS. Note that, for consistency regarding temporal variability, we also calculate this POP annual average from monthly data, not from the daily output that is used for the Lagrangian tracking.

The data from the IC moorings are incorporated in the monthly OSNAP time series that is available from summer 2014–summer 2020 (Fu et al., 2023; Li et al., 2017, 2021; Lozier et al., 2017, 2019). The data (velocity, temperature and salinity) are interpolated on a regular grid along the OSNAP section with a horizontal resolution of 0.25° and a vertical resolution of 20 m. The OSNAP time series combines mooring data with hydrographic sections, ARGO data and satellite altimetry. Further details on the processing can be found in Li et al. (2017). In this study, we only use the OSNAP East section that covers the Irminger Sea and the Iceland Basin.

To investigate the potentially different sources of the two IC cores, their velocity structure in the horizontal and vertical, and the distinguishable properties of each core, need to be properly represented in POP. In Figure 2, we compare velocity, temperature and salinity at the OSNAP East section as simulated by POP (1-year average) with the 2014–2020 mean of the OSNAP fields.

Starting with across-section velocity (Figures 2a and 2b), on the eastern side of the RR at ∼30.5°W the southward flow of the ERRC is clearly identifiable in the simulation and of similar strength as in the observations. On the western flank of the RR (34°- 31°W), POP reproduces the two-core structure of the IC as well as surface-intensified northward velocities, but deep velocities near the top of the RR are stronger than in observations. The location of the IC's western core is slightly more eastward in POP than in OSNAP. This could indicate that the moorings miss part of the western core in the current set-up or that POP overestimates the western core. Also, de Jong et al. (2020) stress the strong spatial variability of the western core on a daily time scale. This difference between POP and OSNAP could therefore also arise from the different time periods considered (1-year mean for POP and 6-year mean for OSNAP). The strong two-core structure of the IC represented by POP agrees well with results from Chafik et al. (2014) using repeat ADCP sections across the Irminger Sea.

Finally, in POP there are strong northward velocities around 37.5°W compared to OSNAP. The velocities east of 34°W in the OSNAP fields are not directly measured, but rather derived from the density gradient between dynamic height moorings and referenced to mean altimetry. Therefore, it is more difficult to compare these velocities to POP. However, the increased northward velocities at 37.5°W resemble the northward branch of the Irminger Gyre from other observations (Våge et al., 2011 their Figures 6a and 8c; Lavender et al., 2000). Even though this additional northward flow cannot be found in some earlier observational studies (Knutsen et al. (2005); Chafik et al. (2014); Rossby et al. (2017)), it has been detected in reanalysis data from 2014 to 2020 (Fried & de Jong, 2022, their Figure 2b).

Overall, velocities of the IC in the POP simulation are slightly higher than in OSNAP, and hence the total volume transport over the whole water column is also higher (13 Sv annual mean from this POP simulation compared to 10.4 ± 4.3 Sv from the IC mooring array (Fried and de Jong (2022), both values computed between 34.2°W and

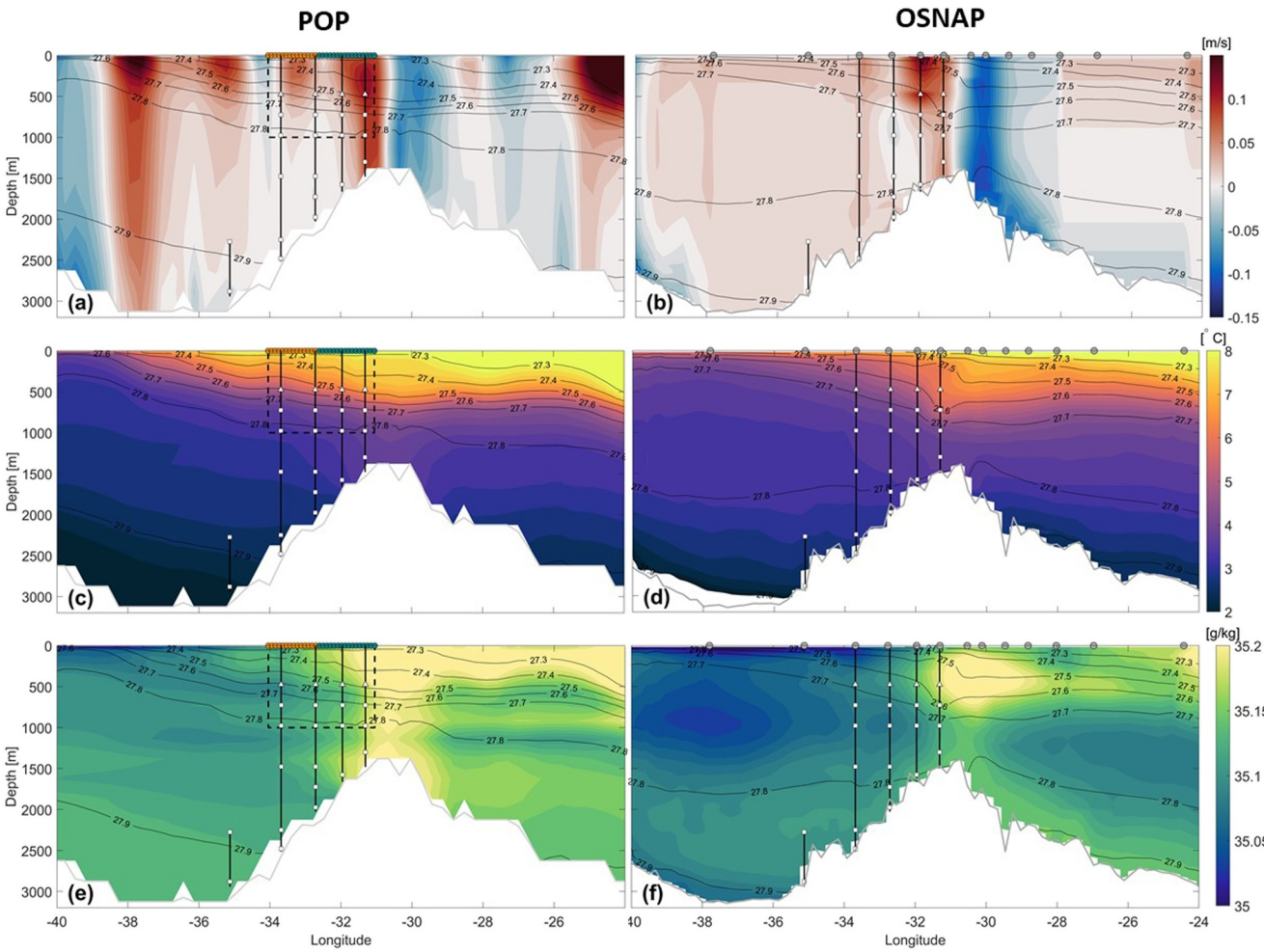

Figure 2. Model comparison aligned with OSNAP East section. Across-section velocities (a), (b), conservative temperature (c), (d) and absolute salinity (e), (f) for annual mean model output from POP (left) and for mean OSNAP climatology averaged over 2014–2020 (right). In all panels, the isopycnals (contours), location of the IC moorings (solid lines) and particle release locations for western (orange) and eastern (blue) are marked. Black dashed box marks the release area and gray solid line marks topography from POP (a, c, e). OSNAP mooring locations are marked with gray dots at the surface (b, d, f); the gray line marks the ETOPO2 bathymetry along the OSNAP East line.

30.7°W). In contrast, POP reproduces the East Greenland Current transport over the upper 500 m very well (−18.2 Sv in POP compared to −18 ± 4 Sv from OSNAP; Le Bras et al., 2018).

A comparison of hydrographic properties, relevant to the differences between the two cores, is shown in Figures 2c–2f. In the Iceland Basin (east of 30.5°W), high temperatures and salinities (>7°C and >35.2 g/kg) are found reaching a depth of ∼300 m in POP. In OSNAP, hydrographic properties are less uniform: the high salinity waters are bound to the ERRC, while waters further west are fresher and colder. At depths exceeding 1,000 m, POP displays higher salinities (35.15 g/kg) than the OSNAP observations (<35.1 g/kg). In the Irminger Sea, POP is colder but saltier at depth than OSNAP, which has a pronounced salinity minimum in the central Irminger Sea (<35 g/kg at 38°W). The $\sigma = 27.8$-isopycnal defines the upper limit of overflow water at depth and is 500 m shallower in POP compared to OSNAP. Within the IC, the eastern core is warmer and saltier than the western core in both the observations and in POP (Figures 2c and 2e). However, the gradient between the western and eastern core is slightly lower in POP than in the observations, and both cores have a warm and salty bias in POP.

For a broader spatial context for the Lagrangian particle study, we compare the horizontal pattern of the circulation in the subpolar gyre (50–70°N, 50–10°W) as simulated by POP to the reanalysis product from CMEMS. The CMEMS product has 1/12° horizontal resolution and 50 vertical levels and hence is comparable in resolution to POP. It uses the NEMO model component as its ocean component and is forced at the surface by ECMWF

ERA-Interim and from first of January 2019 by ERA5 reanalyses. For our comparison, we use monthly output of horizontal velocity, from which we calculate speed and eddy kinetic energy, from 2014 to 2020. A recent comparison of the CMEMS reanalysis to the in-situ ocean observations at the IC mooring array (de Jong et al., 2020; Fried & de Jong, 2022) already showed that reanalysis data reproduces the two-core structure of the IC well for the period 2014–2016. Reanalysis data from 2014 to 2020 exhibits the strong northward flow of the Irminger Gyre at 37.5ºW (Fried & de Jong, 2022, their Figure 2b). Here, we focus on the spatial comparison.

Figure S1 shows surface maps of speed (a), (b) and eddy kinetic energy (c), (d) at 50 m depth from POP (left) and from CMEMS (right). In general, POP has a faster flow field than CMEMS. The ERRC, IC and the EGC are clearly visible in both models and of similar strength. South of ∼57°N the velocities produced by POP are higher. The pathway of the NAC slightly differs compared to CMEMS: a strong north-westward current is present in the central Iceland Basin. The mean surface circulation of POP compares well to circulation presented by Bower et al. (2002) in a Lagrangian model study. The surface eddy kinetic energy (Figure S1c, S1d in Supporting Information S1) is generally of similar magnitude in POP and CMEMS although POP has slightly lower EKE on the East Greenland shelf and in the central Iceland Basin. The differences are most likely related to the 1-year mean from POP that we compare to a 6-year mean from CMEMS which could smoothen over part of the variability.

In summary, despite the discrepancies discussed above, we judge this 1/10° POP simulation is fit for the purpose of this study as it reproduces the two-core structure and the associated differences in properties of these IC cores and the mean flow field in the Irminger Sea.

2.3. Lagrangian Particle Tracking in OceanParcels

We use the Python package OceanParcels (version 2.4.1, Delandmeter & Van Sebille, 2019) as Lagrangian particle tracking software. In OceanParcels, the tracks of virtual particles are calculated using a fourth order Runge-Kutta scheme. We advect particles backwards in time using three-dimensional daily velocity output (u, v, w) from the POP simulation. We update their positions with a time step $\Delta t = 1$ hr and save this information every 2 days. In addition, the temperature and salinity at their updated positions is extracted from the POP output by interpolation and saved. Particles will thus follow the local flow, retaining their buoyancy and moving along isopycnals except at locations with substantial mixing.

We release the particles along a section aligned with the OSNAP East mooring array (Figure 1). It extends far enough westward to encompass the IC (westernmost point: 59.21°N, 34.04°W) and ends at the top of the Reykjanes Ridge (easternmost point: 58.92°N, 31.05°W). We release particles with a horizontal spacing of 6 km (approximately the size of the model grid) and a vertical spacing of 50 m from the surface down to 1,000 m depth, thus capturing the surface-intensified cores of the IC (see Figure 2). As particles move along isopycnals except at locations where substantial mixing takes place, they can reach depths larger than 1,000 m. We categorize the particles as released in the western or eastern core based on the features of the mean velocity field (western core [59.21°N, 34.04°W] to [59.08°N, 32.7°W]; eastern core [59.07°N, 32.6°W] to [58.92°N, 31.05°W]; see Figure 2a).

Particles are released daily over a period of 1 year and tracked backwards in time for a period of 1 year. To be able to do this with the limited POP data set, following for example, Ypma et al. (2019) and Georgiou et al. (2021), we loop the 1-year velocity data from summer to summer.

To justify this approach, we verified that the tracks do not show consistent, large variations from the end of June to the beginning of July attributable to this looping of the velocity data. Further inspection of the tracks revealed particles that unexpectedly stalled within the 1-year time period. Those particles were kept in the data set after cutting the track length to 2 days before the stalling, provided the remaining track length spanned at least 50 days. In Figure S2a in Supporting Information S1 we show the distribution of particle track lengths after these pre-processing steps, highlighting that most tracks are between 50 and 200 days long. We do not find any systematic difference between particle track lengths for eastern and western core (Fig. S2b,c) The cut-off value of 50 days is based on preliminary analyses of the tracks. Since our aim is to study near-field upstream source regions of the two IC cores, thereby distinguishing particles that originate from the Iceland Basin and from the Irminger Sea, tracks need to be sufficiently long to capture a potential crossing of the Reykjanes Ridge. It appeared that more than 90% of the particles that originate from the Iceland Basin travel from the ridge to the release location within the chosen 50-day time span.

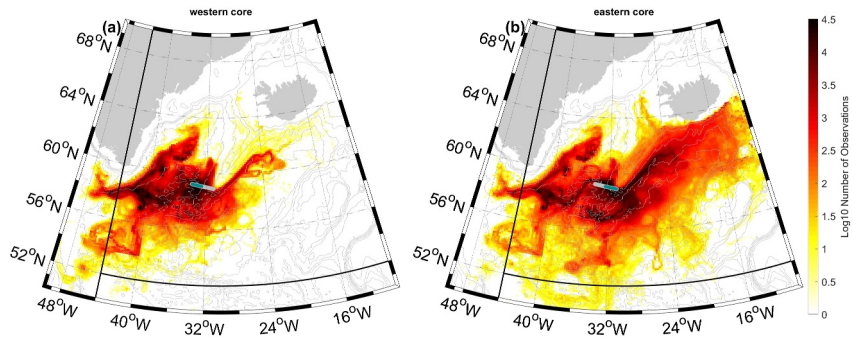

Figure 3. Lagrangian particles density distribution for western and eastern core Particle density distribution of particles seeded in the upper 1000m in the western (a) and eastern (b) core. Particle positions are binned to 0.25° in longitude and 0.125° in latitude. If a particle stays in the lat-lon bin, it is counted again. The thick gray line marks the release locations, the overlaid cyan line marks the western or eastern core, respectively. Black solid lines mark the boundaries used to categorize particles as west of 45°W, south of 52°N, and in the eastern subpolar gyre (see text for details). The model bathymetry is plotted in gray contours with a contour interval of 500 m.

The pre-processed data set contains 207,373 particles in total, of which 95,894 are released in the western core and 111,479 in the eastern core.

3. Main Pathways and Travel Time

For a first impression on pathways to the two IC cores, we compute the density distribution of all particles over the upper 1,000 m for western (Figure 3a) and eastern (Figure 3b) core respectively. To construct this map, particle positions are binned to 0.25° in longitude and 0.125° in latitude where every occurrence of a particle in a lat-lon bin is counted.

There is a clear difference between the distribution for particles backtracked from the two IC cores: for the western core (Figure 3a) the particles density in the Irminger Sea is higher, while for the eastern core (Figure 3b) the particle density is higher in the Iceland Basin. Additionally, particles tracked back from the eastern core span a wider region in the Iceland Basin than those tracked back from the western core. As noted above, even though particle tracks can have different lengths, we did not find a systematic difference between the track lengths for the eastern and western core. The wider spread can therefore not be related to different particle track lengths. From the particle density maps together with particle tracks (not shown) we identify the main following pathways: (a) in the Iceland Basin along the eastern flank of the RR crossing the ridge close to the release location, (b) in the Iceland Basin, along the eastern RR crossing the ridge farther south near the BFZ (57°N) with some particles re-entering the Iceland Basin before reaching the release location and (c) in the Irminger Sea, from the western Irminger Sea off the coast of Greenland and then eastward across the Irminger Sea to the release location. Increased particle density north of the release line may be due to the southward recirculation between the two IC cores (Figure 2) or to mesoscale activity as observed by Fried and de Jong (2022). As Figure 3 shows the density distribution of all particles combined, it obscures if pathways differ depending on release depth. To assess if this is the case, Figure S3 in Supporting Information S1 shows particle density distributions for particles released at 200 m (Figure S3a–S3b in Supporting Information S1) and 1,000 m (Figure S3c–S3d in Supporting Information S1). At depth, the western core is mainly fed from the Irminger Sea with only a very small contribution from the Iceland Basin compared to the eastern core (Figure S3 in Supporting Information S1). Pathways of particles that were released at 1,000 m are more constrained by the topography and originate from deeper parts of both basins (Figure S3c, S3d in Supporting Information S1).

To quantify the number of particles originating from various basins and regions, we first distinguish particle trajectories that originate from within the Irminger Sea and Iceland Basin from those that either come from west of 45°W or from south of 52°N (boundaries marked as black lines in Figure 3) within the 1-year travel time considered.

Of the particles released in the western core, 92% originate in the Irminger Sea and Iceland Basin. The remaining particles (8%) mainly originate from west of 45°W (8%) and a smaller portion from south of 52°N (<1%). For

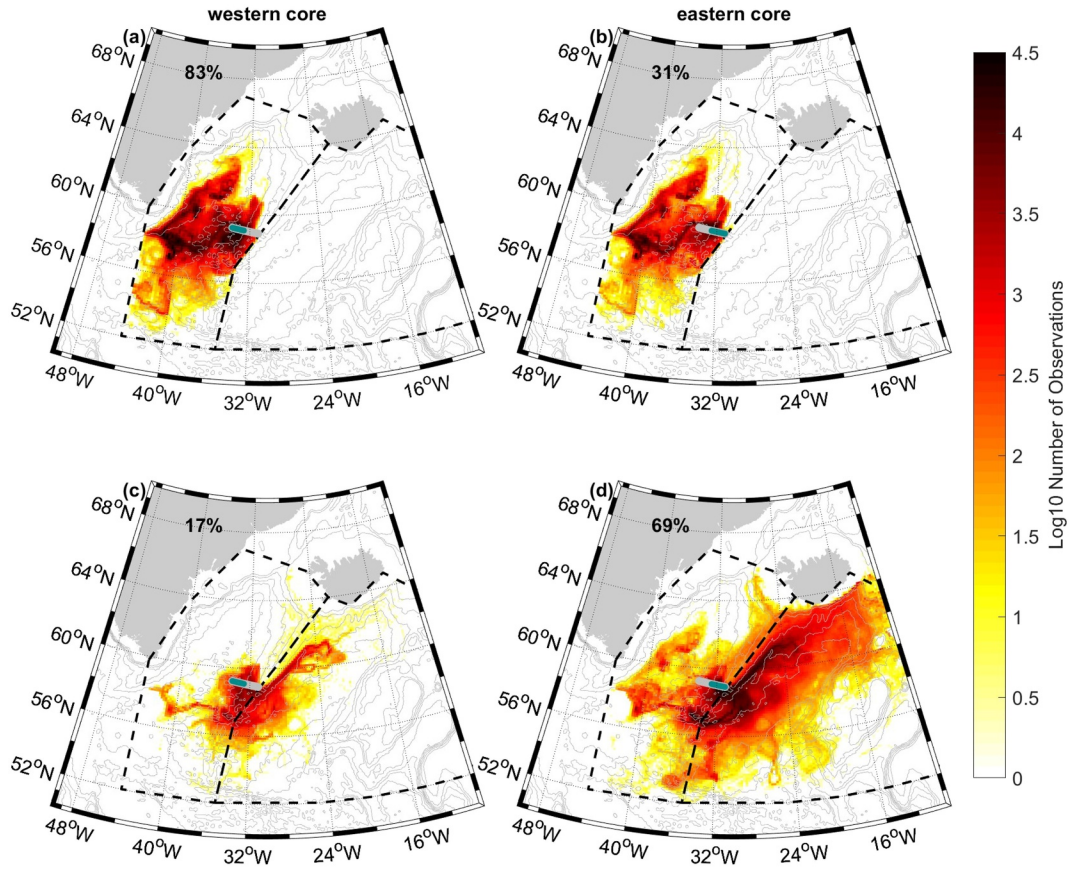

Figure 4. Particle density distribution for Irminger Sea and Iceland Basin As Figure 3 but categorized as particles originating from the Irminger Sea (a), (b) and Iceland Basin (c), (d) for western and eastern core respectively. Dashed lines indicate the boundaries used to classify the particles as coming from a specific region. Percentages in the figure panels refer to the total number of particles originating from either the Irminger Sea or the Iceland Basin for the western (a), (c) and eastern (b), (d) core, respectively.

particles released in the eastern core 97% originate from the Irminger Sea and Iceland Basin. The remaining particles (3%) originate from west of 45°W (3%) and a smaller portion from south of 52°N (<1%). As these contributions from outside the Irminger Sea and Iceland Basin within the considered time frame are so minor, we focus on the particles that originate only from these two basins for the remainder of the study. All percentages mentioned in the following apply to the subset of particles originating from within the area outlined by the black line in Figure 3 (east of 45°W and north of 52°N).

To identify whether particles originate from the Irminger Sea or the Iceland Basin, we define two areas separated by the RR (black dashed lines, Figure 4). The presented numbers are not affected by the different track lengths as the crossing of the RR happens within the first 50 days, which are included in all tracks. Note that particles defined as Irminger Sea particles do not show any appearance in the Iceland Basin through the entire back tracking time period. Within the 1-year tracking time period, 83% of the particles seeded in the western core (Figure 4a) are from the Irminger Sea and 17% are from the Iceland Basin (Figure 4c). For particles seeded in the eastern core 31% are from the Irminger Sea (Figures 4b) and 69% from the Iceland Basin (Figure 4d). Thus, the eastern core contains more than three times as many particles from the Iceland Basin, than the western core. The western core is mainly fed by the Irminger Sea, followed by the Iceland Basin and then the Labrador Sea. The eastern instead is mainly fed from the Iceland Basin, followed by the Irminger Sea and the Labrador Sea. Additionally, the eastern core shows a zonal pathway at BFZ related to the strong zonal (eastward) flow at BFZ (Figure 4d, Figure S1a in Supporting Information S1, see Section 4 for further discussion).

In addition to identifying the main pathways along which waters reach the IC at the release location, we investigate the travel times along these pathways. In Figure S4 in Supporting Information S1, we present the mean

travel time per longitude/latitude bin, that is, how much time particles need on average to travel from that specific location to the release location. Again, we distinguish between the particles from the western core (Figure S4a in Supporting Information S1) and from the eastern core (Figure S4b in Supporting Information S1). To get a robust estimate, we only show bins with a minimum number of 10 particles. It is found that from the central Irminger Sea and the eastern flank of the RR, particles need less than 50 days on average to reach the release location for both cores (Figure S4a, S4b in Supporting Information S1). From the southeastern Iceland Basin as well as from the southern Irminger Sea, particles need the maximum tracking time of 1 year to reach the release location. From BFZ (57°N), particles need between 50 and 100 days. From the northern Irminger Sea (north of 62°N) particles can reach the release location within 100–200 days (Figure S4a, S4b in Supporting Information S1). From Cape Farewell particles can reach the release location within 50 days. The standard deviation of the travel time (not shown) is especially low (<10 days) along the eastern flank of the RR which indicates that this is a very steady pathway to the release location. Overall, mean travel time for both the western and the eastern core is similar for similar pathways. We also show the travel time at 200 and 1,000 m depth (Figure S5 in Supporting Information S1). Differences in the travel time patterns at different depths are minor and follow a general feature of longer travel times for deeper waters, due to lower mean advective speeds.

In summary, within the 1-year tracking time considered here, waters in the IC are mainly supplied by the Irminger and Iceland basins with small contributions from south of 52°N and west of 45°W. The particle density maps show that the waters feeding the two IC cores take similar pathways toward the release location, but that the fraction of particles taking each pathway differs: the western core is predominantly fed by the Irminger Sea and the eastern core by the Iceland Basin.

4. Variability at Reykjanes Ridge

Next, we investigate where particles from the Iceland Basin cross the RR to enter the IC. To this end, we assess where along the RR and when a particle last crosses the ridge before arriving at the release location. We limit our analysis to the latitudes between 56°N and 59.5°N, which seems to be the main crossing area from Figures 4c and 4d. This includes BFZ at ∼57°N and a crossing further north at ∼59°N, both of which have previously been reported as gateways from the Iceland Basin to the Irminger Sea (Koman et al., 2020; Petit et al., 2018, 2019).

Figures 5a and 5b show a histogram of the location where particles cross the RR, for particles feeding the western (a) and eastern (b) core respectively. As the eastern core has more than three times more particles coming from the Iceland Basin toward the release location than the western core (Section 3), the outcomes are presented as the percentage of the total number of particle crossings for that specific IC core. We find that the western core particles have two preferred crossing locations before reaching the release location, at 57°N and at 59°N (Figure 5a), while the eastern core particles display a preference for one location, near 59°N (Figure 5b). More than 60% of the eastern core particles last crossed the ridge between 58.5°N and 59°N. The western core particles generally cross more spread out along the ridge, with around 20% crossing near BFZ (57–57.5°N).

To understand this difference, we show 1-year mean across-ridge velocity (U is rotated by 10° clockwise to get across and along ridge velocities, Figure 5c). The presence of a preferred crossing location at 59°N can be explained by this mean flow, with westward velocities bringing waters from the Iceland Basin to the Irminger Sea. In contrast, the annual mean velocity at BFZ (57°N) is weakly eastward and therefore cannot explain the existence of the second peak in ridge crossings into the Irminger Sea for the western core particles (Figures 5a and 5c). However, the flow at this location exhibits a high temporal variability as already illustrated by the monthly mean fields in Figure S6 in Supporting Information S1. Certain months (e.g., October) exhibit westward velocities that are likely responsible for the particles crossing at BFZ. The constant westward flow north of the maximum particle crossing (Figure 5c) likely feeds the IC north of the chosen release location. Therefore, by the construction of this study it does not result in high particle crossings. The very few particles that do cross north of the release line must enter the IC with a southward flow from the north.

To better understand the temporal variability of the ridge crossings we split the particle crossings by month in which they cross (Figure 6) and, based on the distributions in Figures 5a and 5b distinguish between particles crossing north and south of 58°N. For the western core (Figure 6a), we find a stronger monthly dependency with a peak in July, and only a small number of particles crosses between February and May. As seen in Figure 5a, most particles cross south of 58°N. The small number of particles entering the western core from the Iceland Basin again reflects that nearly all western core particles have their origin in the Irminger Sea. For the eastern core

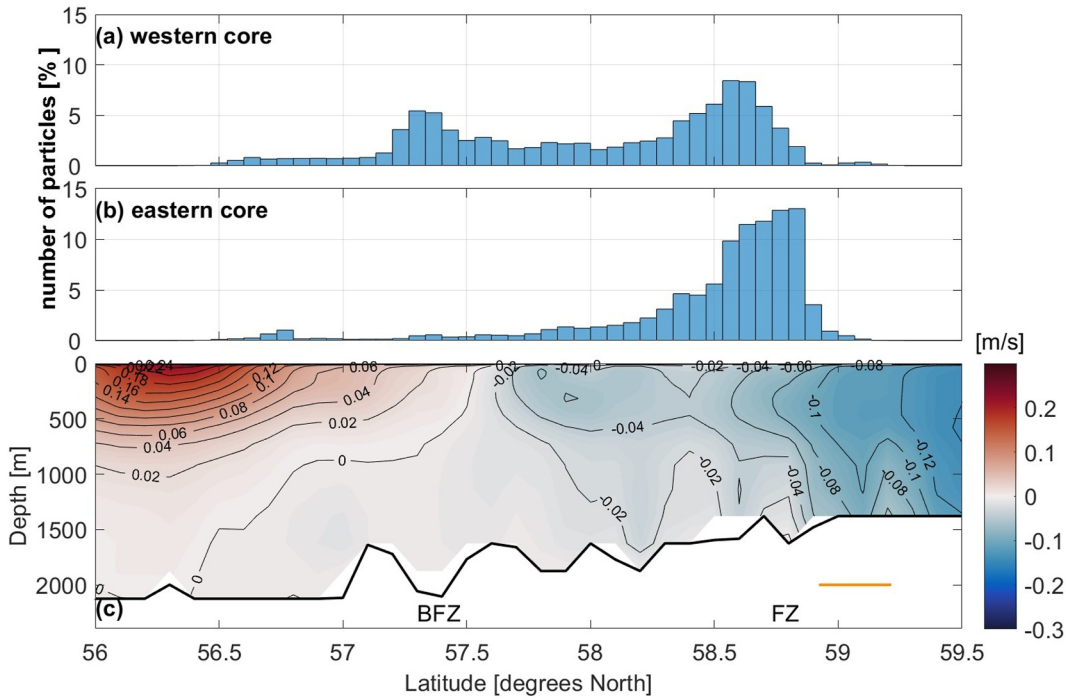

Figure 5. Particles crossing at the Reykjanes Ridge Section (a)**,** (b) Histogram of the fraction of all particles that cross the RR section as a function of latitude, for the western (a) and eastern (b) core [in % of all particles crossing for each core respectively]. (c) One-year mean across-ridge velocity (U, shading, contours) from POP. Ridge topography is indicated by the dark black line; release locations by the orange line; BFZ marks the location of Bight Fracture Zone, FZ the additional Fracture Zone.

(Figure 6b), particles cross in every month but vary in number with a maximum in October and a minimum in February. This can be linked to the variability of the flow field (Figure S6 in Supporting Information S1). In October, the flow field is strongly westward north of 58°N, while in February eastward velocities are present. Additionally, we investigate the particles crossing south of 58°N to investigate whether the crossing at BFZ is

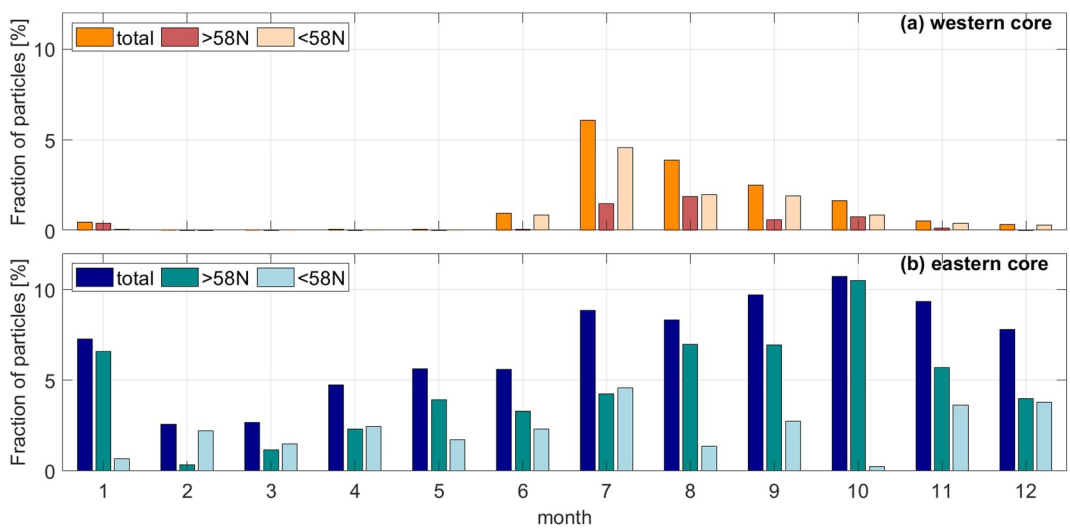

Figure 6. Monthly variability in particle crossings at Reykjanes Ridge. Fraction of particles [in % of the total number of particles crossing] crossing the ridge into the Irminger Sea for particles feeding the western (a) and eastern (b) IC core sorted by month. For each core, we further distinguish the results into particles crossing north and south of 58°N.

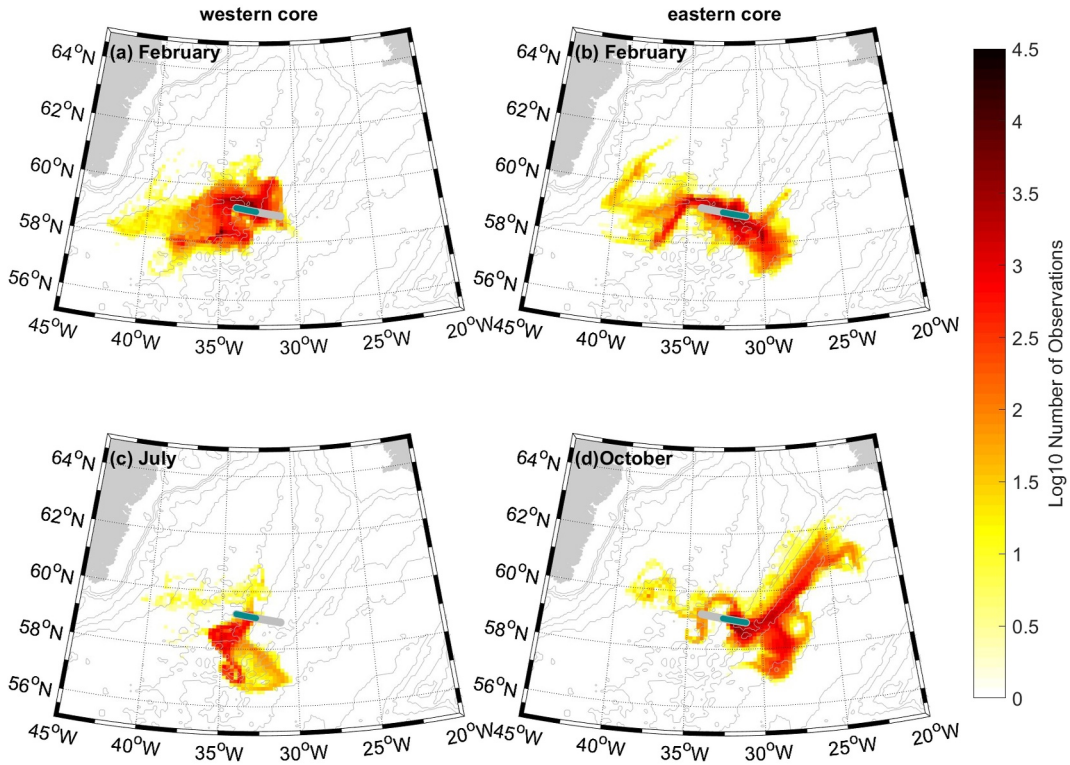

Figure 7. Particle density distribution for months with maximum and minimum number of ridge crossings Particle density distribution calculated from the tracks up to 50 days before reaching the release location for the western (a), (c) and eastern (b), (d) core for February (a), (b) and July (c) and October (d). Model bathymetry is plotted in gray contours every 500 m. The thick gray line marks the release locations, the overlaid cyan line marks the western or eastern core, respectively.

dependent on the month in which they cross. In line with Figure 5b a small fraction of eastern core particles crosses south of 58°N (light blue bars in Figure 6b).

As the ridge crossing locations are close to the release location, it is anticipated that monthly variations in the crossing are linked to the flow conditions in the month a particle was released. On average particles need less than 50 days to travel from the eastern side of the ridge to the release location (Figure S4 in Supporting Information S1). Therefore, we show particle density distributions from the tracks up to 50 days before particles reach the release location classified by release month (Figure 7). We focus on the minimum (February) and maximum (west: July, east: October) that we identified from the fraction of particles crossing the ridge (Figure 6) to investigate potential differences in pathways. In February, particles released in the western core originate from the Irminger Sea instead of the Iceland Basin (Figure 7a). In contrast, the eastern core has a contribution from both basins mostly crossing north of 58°N in line with the flow field (Figure S6h in Supporting Information S1, Figure 7b). In July, particles released in the western core cross the ridge around BFZ with a very small contribution of the central Irminger Sea (Figure S6a in Supporting Information S1, Figure 7c). Eastern core particles released in October mostly originate from the Iceland Basin crossing just south of the release location with a clear pathway along the eastern flank of the RR (Figure S6d in Supporting Information S1, Figure 7d). In addition, we find high particle density away from the ridge highlighting the exchange with the interior Iceland Basin.

In summary, particle crossings at the RR exhibit spatial and temporal variability. Particles mostly cross at 59°N, the western core particles also show an additional crossing location at BFZ. The contribution from particles originating from the Iceland Basin is present throughout the year with variable strength for the eastern core. In contrast, for the western core, there is hardly any contribution from the Iceland Basin between February and May. Thus, we find that the ratio of contribution from the Iceland Basin versus the Irminger Sea for the IC cores varies on a monthly time scale.

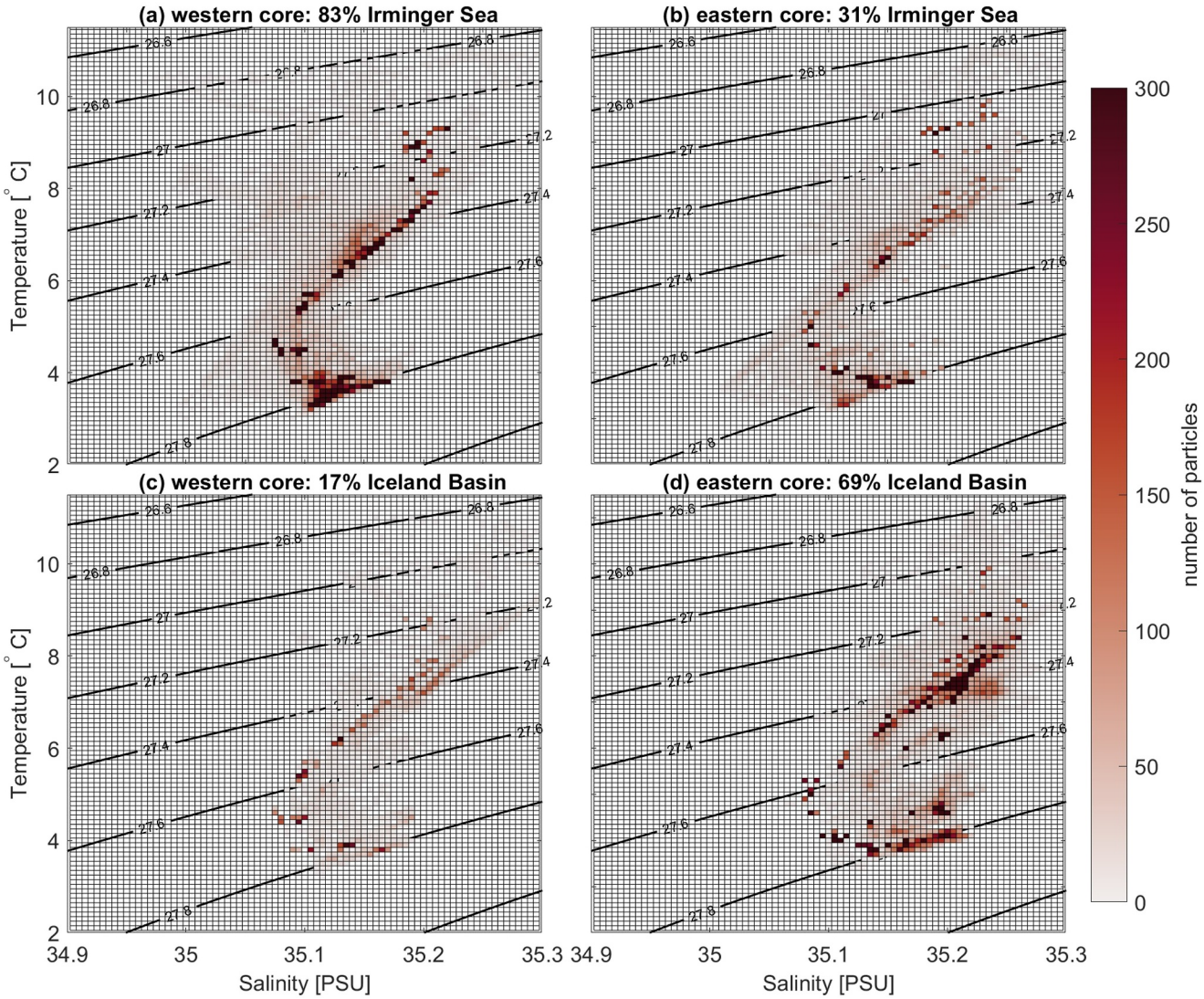

Figure 8. Distribution of TS properties of particles at the release location split by origin Binned distribution of temperature and salinity for particles released in the western (left) and eastern (right) core, originating from the Irminger Sea (a), (b) or Iceland Basin (c), (d). Black solid lines indicate isopycnals. Particles are binned at 0.1°C and 0.005 g kg^{-1} resolution. Percentages in the title indicate number of particles from each respective region.

5. Water Mass Properties of the Two Irminger Current Cores

The previous sections focused on the pathways of the respective IC cores. Now, we investigate the influence of different sources on the water mass properties in the IC cores. The two-core structure of the IC is characterized by the eastern core being warmer and more saline than the western core (Figure 2). In Figure 8 we show the particle density distribution in T-S space at the release location for the western (left) and eastern (right) core split by source region (Irminger Sea Figures 8a and 8b; Iceland Basin Figures 8c and 8d). As expected, the western core consists of more particles with low salinities and cold temperatures (Figures 8a and 8c) compared to the eastern core (Figures 8b and 8d). The eastern core has a higher number of particles lighter than 27.4 kg m^{-3} at salinities higher than 35.2 g kg^{-1} coming from the Iceland Basin (Figure 8d) compared to western core (Figure 8c). In contrast, the western core shows high particle numbers at densities below 27.7 kg m^{-3} (Figure 8a) making it fresher compared to the eastern core (Figure 8b). Hence, particles from the Iceland Basin have similar properties in eastern and western core but are warmer and more saline than those coming from the Irminger Sea.

To investigate changes in TS properties along the pathway, we show the difference in distribution of TS properties of the particles when they are released and 50 days prior to that in Figure S7 in Supporting Information S1.

Particles from the Irminger Sea are denser (mostly colder but also fresher) 50 days before (Figure S7a, S7b in Supporting Information S1). In the Iceland Basin changes are less uniform for both eastern and western core, some particles were slightly fresher and colder (Fig. S7c,d). Particles from the Iceland Basin are slightly lighter, mostly related to higher temperatures (Figure S7c, S7d in Supporting Information S1). Toward the release location particles change their properties due to mixing with the surrounding water masses.

In summary, at the release location particles from the Iceland Basin and Irminger Sea are still distinguishable in properties. Those from the Iceland Basin are warmer and more saline than particles from the Irminger Sea. The difference between the source waters creates the difference in core properties seen in Figures 2c–2e, while the contribution of the Irminger Sea particles to both cores flattens the gradient between the two.

6. Summary and Discussion

In this study, we investigated the pathways to the IC at the OSNAP East line with a focus on the difference between the western and eastern IC core. To this end, we applied Lagrangian particle tracking to a 1/10° model simulation. We first validated this model simulation against observations and an ocean reanalysis product and found reasonably good agreement in terms of the velocity structure of the two IC cores and their respective property differences (Figure 2, S1 in Supporting Information S1).

The model bathymetry at 1/10° resolution is sufficiently detailed to represent the main observed preferential crossing locations at the Reykjanes Ridge. Similarly, the configuration is eddy permitting. While smaller-scale mesoscale variability may be underestimated in POP, the main regions of enhanced EKE are represented (Figure S1c, S1d in Supporting Information S1).

Next, we released particles in the IC at the OSNAP East line and tracked them backwards in time for 1 year. We found that of the particles seeded in the western core 83% originate from the Irminger Sea and 17% from the Iceland Basin (Figures 4a and 4b). In contrast, 31% of the particles seeded in the eastern core originated from the Irminger Sea and 69% from the Iceland Basin (Figures 4c and 4d). This leads to a different composition of water masses at the release line for western and eastern core. The IC's connection to the Iceland Basin corroborates the results by Furey et al. (2001) derived from tracks of RAFOS floats. These were released at the Mid Atlantic Ridge, and circulated cyclonically in the Iceland Basin before they entered the Irminger Sea and partly followed the IC. Petit et al. (2019) investigated the sources of the IC with a budget analysis using hydrographic sections. They found that in addition to the waters from the Iceland Basin, which are responsible for a warming and salinification of the IC, especially the western IC core is fed by cold and fresh waters from the Irminger Sea or Labrador Sea. This close connection of the western core with the Irminger Sea agrees with our study. In contrast, we did not find a close connection to the Labrador Sea, which may be due to the limited (1 year) duration of our particle tracking experiment. We do find slightly increased particle density south of 56°N and west of 40°W (Figure 3a) that may be an indication of this pathway identified by Petit et al. (2019) but the number of particles reaching the IC from that region is very small. On the other hand, the study by Petit et al. (2019) might overestimate the contribution from the Labrador Sea, as it is based on a hydrographic snapshot, and we show in this study that the variability in the circulation can be high.

We identified the pathway along the eastern side of the RR as a fast gateway toward the release location that can be reached within 50 days (Figure S4 in Supporting Information S1). A similarly fast route is from the Irminger Sea along the east Greenland coast and then retroflecting westward toward the release location in the eastern Irminger Sea. This retroflection of waters flowing southward along the east Greenland shelf into the Irminger Sea has been described earlier by Holliday et al. (2007, 2009). High particle density north of the release line could arise from the southward recirculation present at the IC array (Figures 2a and de Jong et al., 2020) or eddy activity in the western core that temporarily increases the southward flow between the two cores (Fried & de Jong, 2022).

We find a strong connection from the Iceland Basin to the Irminger Sea, especially connected to the eastern IC core. Pacini et al. (2020) used hydrographic data from OSNAP moorings in the Irminger Sea and Iceland Basin from 2014 to 2018 to investigate the connection between these parts of the array. They could not find a significant connection between the Iceland Basin and eastern Irminger Sea and concluded that waters are modified by the overlying atmosphere and are therefore hard to track across the ridge (Pacini et al., 2020). However, this might depend on the strength of the wintertime forcing. Convection in the IC itself was exceptionally strong in the winters of 2014/2015 and 2015/2016 (up to 400 m, de Jong et al., 2020) and could have influenced the flow field

and with that the connection between the Irminger Sea and the Iceland Basin that Pacini et al. (2020) refer to. In this study, we showed that indeed many IC particles come from the Iceland Basin. We also showed that the water mass properties of the particles 50 days prior differ to those at the release location. This could explain why Pacini et al. (2020) could not find a connection using hydrographic data.

Our results agree with previous results showing that the main location where waters cross the RR to enter the Irminger Sea is around 59°N (Section 4; Koman et al., 2020; Petit et al., 2018). We find that particles crossing at this location mainly feed the eastern core, and that a secondary peak in particles crossing exists at 57°N, mostly contributing to the western core. The distribution of particles crossings varies by month and might be related to the seasonality of the ERRC. Knutsen et al. (2005) reported a maximum volume transport in autumn using shipboard ADCP data, which is in line with the eastern core's maximum particle number crossing the RR in October. Koman et al. (2020) only find a seasonality in transport on top of the ridge, close to our release location, using mooring data and ARGO observations. The identified variability in the velocity field from POP may be part of the seasonal cycle described by de Jong et al. (2020), who showed a strengthening of the total IC transport in spring. A seasonal cycle in transport could be explained by waters first reaching the eastern core in spring, which increases the density gradient between western and eastern core and with that the volume transport of the IC.

Also, the crossing of particles at BFZ was shown to be controlled by a varying velocity field. We showed that the mean flow in the model at BFZ is slightly eastward (Figure S1a in Supporting Information S1). Using acoustically tracked floats Bower et al. (2002) instead find a westward flow into the Irminger Sea above the 27.5–isopycnal. The model velocity field though does show weakly westward flow at depth in July, September and October (Figure S6 in Supporting Information S1), which supports the findings from Bower et al. (2002). The strong eastward flow in POP at BFZ is in line with observations by Petit et al. (2018). They show a hydrographic section along the RR from 2015 where an eastward flow into the Iceland Basin is present albeit slightly further north than what is found in POP. The eastward flow at BFZ in POP might be a seasonal feature. A field study at BFZ could help verifying whether the eastward flow as shown in POP is realistic. To further investigate the monthly variability of particles entering the Irminger Sea and a potential seasonal cycle related to that, a model study with yearly varying atmospheric forcing would be helpful.

In addition to the pathways, we show that particles originating from the Irminger Sea are fresher and colder than their counterparts originating from the Iceland Basin for both the western and eastern IC core. The properties at the release location therefore depend on the fraction of waters from each basin. Especially in the Irminger Sea we find the particles to be much colder and fresher 50 days before reaching the release location. This shows that over a short distance particles undergo strong mixing. The strong eddying over the ridge will contribute to this mixing and transformation, and with that to the transport variability of the IC, which is a topic for future research. Understanding the interaction of the RR, the IC and the interior Irminger Sea could shed further light on transport variability at the release location.

On interannual to decadal time scales, the variability of the IC transport at the OSNAP East line is influenced by density changes across the whole Irminger Sea, while on shorter time scales it is more related to changes in the local density gradient across the IC itself (Fried & de Jong, 2022). As presented in this study, these changes in the IC density gradient are likely related to the variability in the ratio of waters coming from either the Irminger Sea or the Iceland Basin and specifically the variability at the Reykjanes Ridge (Figures 7 and 8).

For the IC, the traditional view of a boundary current flowing southward along the eastern flank of the Reykjanes Ridge, crossing the ridge and then turning northward along the western flank, only partly holds. This view overlooks the contribution of recirculating water from the Irminger Sea that contributes to both IC cores. Thus, rather than describing the Irminger Gyre as a recirculation of colder Irminger water and a separate IC with warmer Subpolar Mode Water from the Iceland Basin, we must interpret the IC as a two-core system with recirculated Irminger Gyre waters contributing to both cores, but with a strongly increasing contribution of Iceland Basin waters toward the Reykjanes Ridge. Further north the IC will receive additional input of waters from Iceland Basin, which was not considered in this study.

Data Availability Statement

The Lagrangian Particle tracks and corresponding Python code to create them can be downloaded via https://doi.org/10.25850/nioz/7b.b.zf. The underlying POP model data output can be made available upon request. The OSNAP data set can be accessed via https://www.o-snap.org/data-access/. The CMEMS (GLOBAL_REANALYSIS_PHY_001_030) data set can be downloaded via: https://doi.org/10.48670/moi-00021 [Accessed on 02-03-2023].

Acknowledgments
We thank René van Westen and Erik van Sebille from Utrecht University for their help on the Lagrangian particle tracking with OceanParcels. We thank all scientists and mariners involved in the OSNAP project who went to sea to collect the observational data used in this study. MFdJ is financially supported by the Innovational Research Incentives Scheme of the Netherlands Organisation for Scientific Research (NWO) under grant agreement nos. 016. Vidi.189.130.

References

Bower, A. S., Le Cann, B., Rossby, T., Zenk, W., Gould, J., Speer, K., et al. (2002). Directly measured mid-depth circulation in the northeastern North Atlantic Ocean. *Nature*, *419*(6907), 603–607. https://doi.org/10.1038/nature01078

Chafik, L., & Rossby, T. (2019). Volume, heat, and freshwater divergences in the subpolar North Atlantic suggest the Nordic Seas as key to the state of the meridional overturning circulation. *Geophysical Research Letters*, *46*(9), 4799–4808. https://doi.org/10.1029/2019gl082110

Chafik, L., Rossby, T., & Schrum, C. (2014). On the spatial structure and temporal variability of poleward transport between Scotland and Greenland. *Journal of Geophysical Research: Oceans*, *119*(2), 824–841. https://doi.org/10.1002/2013jc009287

Cuny, J., Rhines, P. B., Niiler, P. P., & Bacon, S. (2002). Labrador Sea boundary currents and the fate of the Irminger Sea water. *Journal of Physical Oceanography*, *32*(2), 627–647. https://doi.org/10.1175/1520-0485(2002)032<0627:lsbcat>2.0.co;2

de Jong, M. F., Bower, A. S., & Furey, H. H. (2014). Two years of observations of warm-core anticyclones in the Labrador Sea and their seasonal cycle in heat and salt stratification. *Journal of Physical Oceanography*, *44*(2), 427–444. https://doi.org/10.1175/jpo-d-13-070.1

de Jong, M. F., de Steur, L., Fried, N., Bol, R., & Kritsotalakis, S. (2020). Year-round measurements of the Irminger Current: Variability of a two-core current system observed in 2014–2016. *Journal of Geophysical Research: Oceans*, *125*(10), e2020JC016193. https://doi.org/10.1029/2020jc016193

Delandmeter, P., & Van Sebille, E. (2019). The parcels v2. 0 Lagrangian framework: New field interpolation schemes. *Geoscientific Model Development*, *12*(8), 3571–3584. https://doi.org/10.5194/gmd-12-3571-2019

Fried, N., & de Jong, M. F. (2022). The role of the Irminger Current in the Irminger Sea northward transport variability. *Journal of Geophysical Research: Oceans*, *127*(3), e2021JC018188. https://doi.org/10.1029/2021jc018188

Fu, Y., Lozier, M. S., Biló, T. C., Bower, A. S., Cunningham, S. A., Cyr, F., et al. (2023). Seasonality of the meridional overturning circulation in the subpolar North Atlantic. *Communications earth & environment*, *4*(1), 181. https://doi.org/10.1038/s43247-023-00848-9

Furey, H. H., Bower, A. S., Richardson, P. L., & Woods Hole Oceanographic Institution MA (2001). Warm water pathways in the northeastern North Atlantic ACCE RAFOS float data report.

Georgiou, S., Ypma, S. L., Brüggemann, N., Sayol, J. M., van der Boog, C. G., Spence, P., et al. (2021). Direct and indirect pathways of convected water masses and their impacts on the overturning dynamics of the Labrador Sea. *Journal of Geophysical Research: Oceans*, *126*(1), e2020JC016654. https://doi.org/10.1029/2020jc016654

Gouretski, V., & Koltermann, K. P. (2004). WOCE global hydrographic climatology. *Berichte des BSH*, *35*, 1–52.

Griffies, S. M., Biastoch, A., Böning, C., Bryan, F., Danabasoglu, G., Chassignet, E. P., et al. (2009). Coordinated ocean-ice reference experiments (COREs). *Ocean Modelling*, *26*(1–2), 1–46. https://doi.org/10.1016/j.ocemod.2008.08.007

Hallberg, R. (2013). Using a resolution function to regulate parameterizations of oceanic mesoscale eddy effects. *Ocean Modelling*, *72*, 92–103. https://doi.org/10.1016/j.ocemod.2013.08.007

Holliday, N. P., Bacon, S., Allen, J., & McDonagh, E. L. (2009). Circulation and transport in the western boundary currents at Cape Farewell, Greenland. *Journal of Physical Oceanography*, *39*(8), 1854–1870. https://doi.org/10.1175/2009jpo4160.1

Holliday, N. P., Meyer, A., Bacon, S., Alderson, S. G., & de Cuevas, B. (2007). Retroflection of part of the east Greenland current at Cape Farewell. *Geophysical Research Letters*, *34*(7). https://doi.org/10.1029/2006gl029085

Knutsen, Ø., Svendsen, H., Østerhus, S., Rossby, T., & Hansen, B. (2005). Direct measurements of the mean flow and eddy kinetic energy structure of the upper ocean circulation in the NE Atlantic. *Geophysical Research Letters*, *32*(14). https://doi.org/10.1029/2005gl023615

Koman, G., Johns, W. E., & Houk, A. (2020). Transport and evolution of the East Reykjanes Ridge Current. *Journal of Geophysical Research: Oceans*, *125*(10), e2020JC016377. https://doi.org/10.1029/2020jc016377

Krauss, W. (1995). Currents and mixing in the Irminger Sea and in the Iceland basin. *Journal of Geophysical Research*, *100*(C6), 10851–10871. https://doi.org/10.1029/95jc00423

Large, W., & Yeager, S. G. (2009). The global climatology of an interannually varying air–sea flux data set. *Climate Dynamics*, *33*(2–3), 341–364. https://doi.org/10.1007/s00382-008-0441-3

Large, W. G., McWilliams, J. C., & Doney, S. C. (1994). Oceanic vertical mixing: A review and a model with a nonlocal boundary layer parameterization. *Reviews of Geophysics*, *32*(4), 363–403. https://doi.org/10.1029/94rg01872

Lavender, K. L., Davis, R. E., & Owens, W. B. (2000). Mid-depth recirculation observed in the interior Labrador and Irminger seas by direct velocity measurements. *Nature*, *407*(6800), 66–69. https://doi.org/10.1038/35024048

Le Bras, I. A. A., Straneo, F., Holte, J., & Holliday, N. P. (2018). Seasonality of freshwater in the East Greenland current system from 2014 to 2016. *Journal of Geophysical Research: Oceans*, *123*(12), 8828–8848. https://doi.org/10.1029/2018jc014511

Lherminier, P., Mercier, H., Gourcuff, C., Alvarez, M., Bacon, S., & Kermabon, C. (2007). Transports across the 2002 Greenland-Portugal Ovide section and comparison with 1997. *Journal of Geophysical Research*, *112*(C7). https://doi.org/10.1029/2006jc003716

Li, F., Lozier, M. S., Bacon, S., Bower, A. S., Cunningham, S. A., De Jong, M. F., et al. (2021). Subpolar North Atlantic western boundary density anomalies and the meridional overturning circulation. *Nature Communications*, *12*(1), 3002. https://doi.org/10.1038/s41467-021-23350-2

Li, F., Lozier, M. S., & Johns, W. E. (2017). Calculating the meridional volume, heat, and freshwater transports from an observing system in the subpolar North Atlantic: Observing system simulation experiment. *Journal of Atmospheric and Oceanic Technology*, *34*(7), 1483–1500. https://doi.org/10.1175/jtech-d-16-0247.1

Lozier, M. S., Bacon, S., Bower, A. S., Cunningham, S. A., de Jong, F. M., de Steur, L., et al. (2017). Overturning in the Subpolar North Atlantic Program: A new international ocean observing system. *Bulletin of the American Meteorological Society*, *98*(4), 737–752. https://doi.org/10.1175/BAMS-D-16-0057.1

Lozier, M. S., Li, F., Bacon, S., Bahr, F., Bower, A. S., Cunningham, S. A., et al. (2019). A sea change in our view of overturning in the subpolar North Atlantic. *Science*, *363*(6426), 516–521. https://doi.org/10.1126/science.aau6592

Mercier, H., Lherminier, P., Sarafanov, A., Gaillard, F., Daniault, N., Desbruyères, D., et al. (2015). Variability of the meridional overturning circulation at the Greenland–Portugal OVIDE section from 1993 to 2010. *Progress in Oceanography*, *132*, 250–261. https://doi.org/10.1016/j.pocean.2013.11.001

Pacini, A., & Pickart, R. S. (2023). Wind-forced upwelling along the West Greenland Shelfbreak: Implications for Labrador Sea water formation. *Journal of Geophysical Research: Oceans*, *128*(3), e2022JC018952. https://doi.org/10.1029/2022jc018952

Pacini, A., Pickart, R. S., Bahr, F., Torres, D. J., Ramsey, A. L., Holte, J., et al. (2020). Mean conditions and seasonality of the west Greenland boundary current system near cape farewell. *Journal of Physical Oceanography*, *50*(10), 2849–2871. https://doi.org/10.1175/jpo-d-20-0086.1

Petit, T., Lozier, M. S., Josey, S. A., & Cunningham, S. A. (2020). A new paradigm for Atlantic Ocean deep water formation. *Geophysical Research Letters*, *47*(22). https://doi.org/10.1029/2020GL091028

Petit, T., Mercier, H., & Thierry, V. (2018). First direct estimates of volume and water mass transports across the Reykjanes Ridge. *Journal of Geophysical Research: Oceans*, *123*(9), 6703–6719. https://doi.org/10.1029/2018jc013999

Petit, T., Mercier, H., & Thierry, V. (2019). New insight into the formation and evolution of the East Reykjanes Ridge Current and irminger current. *Journal of Geophysical Research: Oceans*, *124*(12), 9171–9189. https://doi.org/10.1029/2019jc015546

Pickart, R. S., Spall, M. A., Ribergaard, M. H., Moore, G. K., & Milliff, R. F. (2003). Deep convection in the Irminger Sea forced by the Greenland tip jet. *Nature*, *424*(6945), 152–156. https://doi.org/10.1038/nature01729

Reverdin, G., Niiler, P. P., & Valdimarsson, H. (2003). North Atlantic surface ocean currents. *Journal of Geophysical Research*, *108*(3002), 10–1029. https://doi.org/10.1029/2001jc001020

Rossby, T., Reverdin, G., Chafik, L., & Søiland, H. (2017). A direct estimate of poleward volume, heat, and freshwater fluxes at 59.58N between Greenland and Scotland. *J. Geophys. Res. (Oceans)*, 122. https://doi.org/10.1002/2017JC012835

Våge, K., Pickart, R. S., Sarafanov, A., Knutsen, Ø., Mercier, H., Lherminier, P., et al. (2011). The Irminger Gyre: Circulation, convection, and interannual variability. *Deep Sea Research Part I: Oceanographic Research Papers*, *58*(5), 590–614. https://doi.org/10.1016/j.dsr.2011.03.001

van Aken, H. M., de Jong, M. F., & Yashayaev, I. (2011). Decadal and multi-decadal variability of Labrador Sea Water in the north-western North Atlantic Ocean derived from tracer distributions: Heat budget, ventilation, and advection. *Deep Sea Research Part I: Oceanographic Research Papers*, *58*(5), 505–523. https://doi.org/10.1016/j.dsr.2011.02.008

Weijer, W., Maltrud, M. E., Hecht, M. W., Dijkstra, H. A., & Kliphuis, M. A. (2012). Response of the Atlantic Ocean circulation to Greenland Ice Sheet melting in a strongly-eddying ocean model. *Geophysical Research Letters*, *39*(9). https://doi.org/10.1029/2012gl051611

Ypma, S. L., Brüggemann, N., Georgiou, S., Spence, P., Dijkstra, H. A., Pietrzak, J. D., & Katsman, C. A. (2019). Pathways and watermass transformation of Atlantic Water entering the Nordic Seas through Denmark Strait in two high resolution ocean models. *Deep Sea Research Part I: Oceanographic Research Papers*, *145*, 59–72. https://doi.org/10.1016/j.dsr.2019.02.002